J Therm Anal Calorim
DOI 10.1007/s10973-017-6531-x

Synthesis, thermoanalytical and spectroscopic characterization of newly synthesized macrocyclic complexes of thallium(III) and tin(IV)

Sapna Katoch[1] · Gauri D. Bajju[1] · Gita Devi[1] · Altaf Ahmed[1]

Received: 2 November 2016 / Accepted: 4 June 2017

Abstract Spectroscopic, thermal and fluorescence properties of various thallium and tin complexes, X-Tl(III)t(4-Y)PP and X-Sn(IV)t(4-Y)PP where X = 5-SO_3H-2-$OHOC_6H_4$,(5-SSA); 5-Cl-2-$OHOC_6H_4$,(5-CSA); and 5-NH_2-2-$OHOC_6H_4$,(5-NSA) and Y = –Cl, –OCH_3, are investigated in detail. Analysis of the spectral data [IR, UV–Vis and NMR (^{1}H and ^{119}Sn)] of complexes suggests that the two trans-axial ligands are strongly bound in a symmetric manner at the tin center in these complexes. Whereas the absorption and emission studies of thallium complexes characterized the sitting-Atop (SAT) feature of the complexes, the fluorescence lifetime of the tin complexes is found to be higher than thallium complexes. The structure and morphology of complexes were studied by X-ray powdered diffraction analysis. From the X-ray diffractograms, it could be revealed that the complexes are crystallized in mixed crystalline forms. Thermal studies of these porphyrins were carried out in an argon atmosphere from room temperature to 800 °C using thermal analyzer. Evaluation of the thermal analysis of the two metal complexes reveals that the tin(IV) porphyrin complexes are more stable than thallium(III) complexes. Some of the synthesized complexes of thallium and tin have been screened for biological activity against *B. subtilis*, *M. luteus*, *S. aureus*, *P. florescens and E. coli* by agar well diffusion methods that were found to be inactive against bacterial strains.

Graphical Abstract

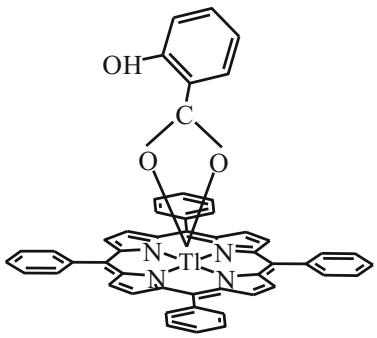

Chemical structure of X-Tl(III)t(4-Y)PP

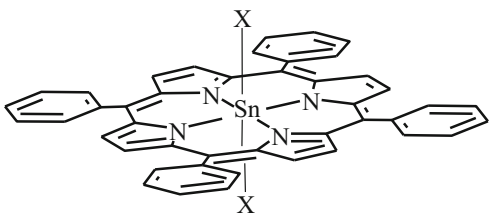

Chemical structure of X-Sn(IV)t(4-Y)PP

X= 5-SO_3H-2-$OHOC_6H_4$,(5-SSA); 5-Cl-2-$OHOC_6H_4$,(5-CSA); and 5-NH_2-2-$OHOC_6H_4$,(5-NSA)

✉ Gauri D. Bajju
gauribajju@gmail.com

[1] Department of Chemistry, University of Jammu, Jammu 180006, India

Keywords Fluorescence · Lifetime · Spectral properties · Thermal studies · XRPD

Published online: 20 June 2017

Introduction

The current interest in coordination chemistry of synthetic macrocycles increases from the facts that among the most important biological compounds are those that contain metal ions with the naturally occurring macrocycles, e.g., porphyrins, the chlorophylls and the corrins [1]. Being one of the vital molecules in many biological processes, polydentate ligand porphyrins and their metalloderivatives have been artificially synthesized, in part associated with mimicking the unusual spectral, redox, kinetic and/or thermodynamic behavior commonly displayed by nature's macrocycles [2] and also for the development of new macrocyclic systems for use in medicine, metal-ion discrimination, metal-ion catalysis, organic synthesis and analytical processes [3–5]. The thermal and chemical stability of metalloporphyrins make them attractive building blocks for the molecular engineering of microporous (i.e., pores with diameters less than 20 Å) framework solids [6] which also often show enhanced resistance to degradation, high thermal stabilities and inertness to acids and alkalis when compared with their metal-containing open-chain analogs.

Tin porphyrins are significant and historically important compounds, for their remarkable combination of chemical and spectroscopic properties, as well as for their numerous practical applications, in medicine [7] and in catalysis [8]. Tin(IV) porphyrins have been extensively studied in biomedical and photocatalytic applications, including splitting of water for the production of hydrogen. They are very stable, easy to synthesize, diamagnetic and usually six-coordinated with trans-diaxial ligands [9]. Although the chemistry of a wide variety of metalloporphyrins has been studied in detail, thallium(III) porphyrins have received little attention. Thallium, being heavy metal, imparts several properties of interest in porphyrin macrocycle receiving nowadays a considerable interest as active materials for OL (optical linear) devices for their capability of absorbing intense radiations (in the order of several megawatts per square meter), in the VIS/NIR spectral range in a reversible fashion with no severe modifications of their optical and chemical properties [10]. The nonplanar distortions of tetrapyrroles that occur naturally in proteins can be induced in model porphyrins by substantial steric crowding at the periphery and by inserting heavy metals like thallium(III) into the core [11]. These distortions have been shown to modulate the photophysical and chemical properties of the chromophores and are believed to be responsible, at least in part, for the various functions and reactivity of chemically similar tetrapyrrole pigments found in nature. This state of development has prompted us to synthesize thallium porphyrins that easily bind various O/N donor ligands to the sixth position, which is the only position available, and enables us to investigate the effects of axial ligand coordination.

Herein, we wish to report on a family of thallium and tin porphyrins that binds the axial ligands strongly enough to be isolable in the solid state and also to scrutinize the effect of axial ligand coordination on the electronic structure and geometry of the macrocycles. This objective has been achieved successfully by using 5,10,15,20-*p*-substituted tetraphenyl porphyrins (*tx*-H_2TPP,x –Cl, –OCH_3) as a porphyrin macrocycle. The presence of four bulky groups at the meso-positions severely distorts the porphyrin geometry and provides an interesting modulation of the macrocycle properties. We also investigate the effects of the macrocycle deformations on the metal centers in order to understand the effects of similar distortions in biology and their thermal stability.

Experimental

Material

The high-purity reagents were commercially purchased from Merck ($SnCl_2{\cdot}2H_2O$), Acros organics $Tl(OAc)_3$, Himedia (*p*-methoxy benzaldehyde, *p*-chlorobenzaldehyde) and were used as received without further purification.

Instrument

UV–visible spectra were recorded on UV/VIS spectrophotometer model T90 and UV-2600 spectrophotometer Shimadzu in the range 350-700 nm using 10^{-4} and 10^{-5} M concentrations for each porphyrin and their corresponding metallated and axially ligated complexes. Infrared analysis of solid porphyrins was recorded on PerkinElmer-spectrum 400 FTIR spectrophotometer using KBr pellets in the range of 4000–400 cm^{-1}. The ^{1}H NMR spectra were recorded on a Bruker Avance II 400 N (400 MHz) using tetramethylsilane as internal standard and $CDCl_3$ as a solvent. ^{119}Sn NMR and ^{204}Tl spectra were recorded on a Bruker 400(L) MHz spectrometer instrument using tetramethyl tin and $Tl^{III}(NO_3)_3$, respectively, as standard using $CDCl_3$ as solvent. TG and DTA were recorded on thermal analyzer, PerkinElmer, model STA-6000 using dry samples at the heating rate of 10 °C min^{-1} in an argon atmosphere from room temperature to 900 °C. The phase and size of the as-prepared samples were determined from powder X-ray diffraction (XRPD) using D8 X-ray diffractometer (Bruker) at a scanning rate of 12 °C min^{-1} in the 2θ range from 10° to 70°, with Cu Kα radiation ($\lambda = 0.15405$ nm). The photoluminescence emission spectra were recorded at room temperature using Agilent Cary Eclipse fluorescence

spectrophotometer equipped with xenon lamp as the excitation source. Lifetime of luminescent nanospheres was measured from fluorescence lifetime measuring system Horiba, Model no: Delta Flex-01-NL.

Synthesis and spectral data of ligands and complexes

5,10,15,20-meso-tetra(p-methoxyphenyl) porphyrin [H_2t(p-OCH_3)PP], P1

4-Methoxybenzaldehyde (0.004 mol) was added to 12 mL of propionic acid. Pyrrole (0.004 mol) was added slowly to the above refluxing mixture. The reaction mixture was refluxed for 40 min and then cooled to the room temperature. The purple precipitation was filtered off and washed with a minimal amount of methanol and then dried. The material was dissolved in a minimal amount of chloroform and chromatographed on a column of basic alumina using chloroform as the eluant. The first band is pink which contains pure P1. The material was collected and taken to dryness under vacuum on a rotary evaporator.

5,10,15,20-meso-tetra(p-chlorophenyl) porphyrin [H_2t(p-Cl)PP], P2

4-Chlorobenzaldehyde (0.004 mol) was added to 12 mL of propionic acid. Pyrrole (0.004 mol) was added slowly to the above refluxing mixture. The reaction mixture was refluxed for 40 min and then cooled to the room temperature. The purple precipitation was filtered off and washed with a minimal amount of methanol and then dried. The material was dissolved in a minimal amount of chloroform and chromatographed on a column of alumina using chloroform as the eluant. The first band is pink which contains P2. The material was collected and taken to dryness under vacuum on a rotary evaporator.

Synthesis of aquo-meso-(5,10,15,20-tetraarylporphyrinato)thallium(III)hydroxide, (OH)(H_2O)Tlt(4-Y)PP] [Y: –OCH_3, –Cl] [TlP1,TlP2]

A mixture of porphyrins 0.0068 mmol in CH_2Cl_2 (10 mL) and $Tl(OAC)_3$ 0.12 mmol in MeOH (2.5 mL) was refluxed for 1 h. After concentration, the residue was dissolved in $CHCl_3$, dried with anhydrous Na_2SO_4 and filtered. The filtrate was concentrated and recrystallized from CH_2Cl_2–MeOH (1:5 v/v) yielding purple solid of complex (0.037 mmol, 55%) which was again dissolved in CH_2Cl_2-ether (1:1 (v/v)] and layered with MeOH to get purple crystals of thallium(III) porphyrins.

General synthesis of dihydroxoporphyrinatotin(IV) [SnP1, SnP2]

A sample of porphyrin (59 μmol) was dissolved in 10 mL of chloroform in a one-neck round bottom flask. The solution of $SnCl_2{\cdot}2H_2O$ (0.59 mmol) in 10 mL of ethanol was added to it, and the reaction mixture was stirred at refluxing temperature. The porphyrin solution turned green on addition of $SnCl_2{\cdot}2H_2O$. The progress of the reaction was monitored by TLC analysis and absorption spectroscopy. The metallation was completed in 4 h as judged by absorption spectroscopy. Triethylamine (0.5 mL) was added to the reaction mixture, and the reaction mixture was stirred for an additional 5 min. The solvent was removed on rotary evaporator, and crude compound was subjected to alumina column chromatographic purification. The residual unreacted free-base porphyrin was collected first with CH_2Cl_2, and the desired dihydroxoporphyrinatotin(IV) was eluted with CH_2Cl_2/1–2% CH_3OH. The solvent was removed on rotary evaporator and afforded the pure Sn(IV) porphyrin as purple solid [10].

Synthesis of axially ligated Tl(III) porphyrins: XTl(III)t(4-Y)PP [X: different salicylates]

(OH)(H_2O)Tl(III)t(4-Y)PP 0.15 mmol in 30 mL $CHCl_3$ was treated with respective salicylates 0.56 mmol in 25 mL CH_3OH and stirred under reflux for 12 h. After concentration, the mixture was dissolved in minimum quantity of CH_2Cl_2 and extracted four times with distilled water to remove excess unreacted salicylates. The resulting solution was then filtered through anhydrous Na_2SO_4 in order to remove water molecule. The CH_2Cl_2 layer was then concentrated to dryness, producing purple prism. The same procedure was applied for the synthesis of all axially ligated complexes of thallium porphyrins.

Synthesis of axially ligated Sn(IV) porphyrins: Sn(IV)($X)_2$t(4-Y)PP [X: different salicylates]

Trans-dihydroxo(meso-tetraphenylporphyrinato)tin(IV) (0.13 mmol) prepared above and salicylates (0.26 mmol) were dissolved in anhydrous CH_2Cl_2 (20 mL).The reaction mixture was stirred at room temperature. After 24 h, the solution was filtered through filter paper. The solvent of the filtrate was evaporated under reduced pressure to give a crude product. It was then recrystallized from CH_2Cl_2/CH_3CN solution to afford crystalline solids of the desired compound.

Results and discussion

Ultraviolet studies

The absorption spectral data of all the *p*-substituted porphyrin, its metal complexes and corresponding axially ligated complexes in methanol are summarized in Table 1.

Both the Soret and Q-bands of the two *p*-methoxy-substituted porphyrins are red-shifted compared with *p*-chlorophenylporphyrin. The broadening and red shifting of the absorption bands are usually an indicator of mixing with the intramolecular charge-transfer character in π–π* absorption bands. Further, the metallated and axially ligated complexes in case of thallium complexes also exhibited prominent red shift in their spectra according to the larger out of plane distance in the case of TlP2 and even the axially ligated complexes resulting in the higher distortion of the porphyrin ligand. According to our observations from the literature, these spectral features are unambiguously characteristic for OOP or SAT complexes, confirming the expectations based on the size (95 pm ionic radius) of Tl(III) ion [12, 13]. Whereas in case of tin complexes, there is a marginal red shift in the absorption spectrum of SnP2 as well as in the axially ligated derivatives in methanol media.

Table 1 Absorption data of free base, metallated porphyrins and axially ligated porphyrins

	B-band λ_{max}/nm	Q-bands λ_{max}/nm
P1	418	516, 546, 590, 648
P2	413	511, 543, 586, 647
TlP1	426	526, 562, 596
TlP2	424	519, 554, 594
5-SSATlP1	436	568, 669
5-SSATlP2	434	563, 671
5-CSATlP1	434	562, 663
5-CSATlP2	433	560, 659
5-NSATlP1	436	563, 660
5-NSATlP2	433	562, 659
SnP1	422	558, 598
SnP2	420	557, 596
5-SSASnP1	427	562, 652
5-SSASnP2	426	561, 650
5-CSASnP1	428	562, 657
5-CSASnP2	427	560, 649

IR spectra

The characteristic infrared absorption bands of the free ligands and four complexes are illustrated in Table 2. All the free ligands exhibited very sharp peak at 3315–3317 cm^{-1} indicating the presence of NH group which is found absent in the corresponding metalloporphyrins. The bands observed at 3640–3643 cm^{-1} corresponds to the stretching vibration of OH groups at the axial position in the metalloporphyrins [14], and the aromatic C–H appears at 3055 cm^{-1}. The symmetric (υ_{sym}) and asymmetric (υ_{asym}) COO bands observed at 1583 and 1479 cm^{-1} in tin complexes bound in the unidentate mode and shift to the lower frequency when compared to the free ligand [15].The bands in the region 1720–1724 cm^{-1} are assigned to the C=O group of salicylates in thallium complexes. The band at 1606 and 1633 cm^{-1} is assigned to the asymmetric vibration of C=O bond in the bidentate mode of salicylates in thallium complexes [16]. The band appearing at 1463 cm^{-1} is assigned to the symmetric (υ_{sym}) vibration of C=O bond in bidentate mode. In addition, the peak at 1179 indicates the vibration band due to C–N stretching and band at 1329 cm^{-1} corresponds to the C=N moiety. Meanwhile, the low frequency absorptions at 430–470 cm^{-1} correspond to the ν(M–O) also suggest that the oxygen atoms from the carboxylate group are coordinated to metal ions. Furthermore, the axially ligated complexes also showed the band corresponding to the OH group giving confirmation that ligation occurs through COO group in both metal complexes.

NMR studies

^{1}H NMR spectra of the free bases P1 and P2, their Tl(III) and Sn(IV) complexes and the corresponding axially ligated complexes in $CDCl_3$ are discussed. All complexes exhibit ^{1}H NMR features characteristic for diamagnetic compounds. The free-base porphyrins exhibited signal at −2.73 ppm related to NH protons and disappear in the corresponding metal derivatives and their axially ligated derivatives. Free-base porphyrins showed singlet at 8.91–8.93 ppm corresponding to the β-pyrrole hydrogens and peaks in the region 7.22–7.24 ppm corresponding to the phenyl hydrogens. In general, NMR is quite informative for confirming the metallation and axial ligation. The eight β-pyrrole protons which appear as singlet in metal-free-base porphyrin appeared as one strong signal surrounded by small satellite peaks in Sn(IV) derivatives [17] giving confirmation for metallation. Furthermore, the β-pyrrole protons were downfield shifted in metalloporphyrins and in the final complexes containing axial ligands compared to free-base porphyrins. However, axially ligated derivatives exhibited signals in the upfield region in the range 6.00–7.00 ppm due to ring current effect in both metal complexes. ^{205}Tl NMR spectra of 5-SSATlP1 when recorded in $CDCl_3$ exhibit a sharp resonance at δ 2629.629 ppm which confirms the presence of Tl(III) ion

Table 2 Important IR absorption bands for the ligand and metal complexes

Compounds	ν(O–H)/ cm^{-1}	ν(N–H)/ cm^{-1}	ν(C–H) asym/ cm^{-1}	ν(sp^3-CH)	ν(=C–H) sym	ν(C=N)/ cm^{-1}	ν(C–N)/ cm^{-1}	ν(C=C)/ cm^{-1}	ν(C=O)	ν(M–O)/ cm^{-1}
P2		3317	2958	2852	2922	1350	1184	1558	–	–
TlP2	3523	–	2962	2850	2926	1333	1184	1552	–	488
5-CSATlP2	3464	–	2962	2843	2923	1328	1178	1513	1723	462
5-NSATlP2	3454	–	2962	2842	2922	1326	1179	1511	1720	472
SnP2	3643	–	2960	2850	2924	1348	1255	1534	–	473
5-CSASnP2	3749	–	2962	2845	2900	1355	1253	1529	1674	472
	3635									
	3533									
5-NSASnP2	3749	–	2960	2843	2918	1353	1252	1525	1670	473
	3636									
	3544									

in the complex. ^{119}Sn NMR spectral signal of the tin complexes in the range δ 500 to −1500 ppm was obtained, supporting hexacoordination of the tin atom and comparable to values previously published for closely related compounds. In the absence of salicylate, a single NMR resonance band is observed for tin, centered at −587 to −590 ppm relative to tetramethyltin (in $CDCl_3$) [2]. In the synthesized tin complex 5-NSASnP1, the band is observed at δ −629.462 ppm and hence confirms that both axial position can be readily displaced by salicylates. These upfield shifts are expected in the light of the increase in electron density around the tin center by the coordinated carboxylate groups of the salicylate.

Thermal decomposition processes of the complexes

5-CSATlP2

The thermal behavior of the synthesized complexes was studied to establish different decomposition process and to confirm the proposed stoichiometry. The endo- and exothermic peaks are observed in DTA curves and are explained with TG curves. The thermal decomposition of the complexes takes place in four stages (Fig. 1). The TG curve reveals that the complexes undergo complete decomposition up to 800 °C, and the DSC curve shows that the complex decomposes in four stages at 148, 247.2, 384.9 and 503.7 °C. In the first stage of thermal dehydration of the complex takes place in between 90 and 200 °C with a mass loss of 1.7% corresponds to the removal of one water molecule. In the second stage, mass loss of 66.8% corresponds to the decomposition of axial ligand, the four mesophenyl rings and two pyrrole rings, as indicated by the exothermic peak at 247.2 °C. The third stage corresponds to the decomposition of two remaining pyrrole rings corresponding to the mass loss of 12.5% in the temperature range of 250–385 °C. This pattern is supported by the DTA curve with exothermic peak at 384.9 °C. In the last stage, remaining moiety, i.e., thallium metal undergoes decomposition with a mass loss of 19.2% and it was compared with theoretical mass value which was found correct. The upper decomposition temperatures of the complexes are all higher than those of the ligands and their metallated derivatives, which indicate that the stability of the complexes is higher than that of the precursors.

5-CSASnP2

Simultaneous TG and DTA curves for the complex are recorded and are shown in Fig. 2. Thermal analysis of the complex 5-CSASnP2 shows that the complex decomposes through four steps. In the first step, mass loss in the temperature range 100–136 °C is due to the dehydration (loss of one water molecule). The second step 136–240 °C with net mass loss of 22.56% corresponded to the elimination of one axial ligand and one chlorophenyl moiety and is indicated by the DTA curve at 237.15 °C. The next step involves the decomposition of 5.04% corresponded to the elimination of CO_2 and Cl species. The third step involves the decomposition of 34.34% in the temperature range of 355–620 °C corresponded to the three chlorophenyl rings and C_6H_5O species. The next step (620°–891°) had a net mass loss of 10.0% and corresponded to the decomposition of the two pyrrole rings and then no more mass loss is observed. The remaining residue mass (26.86%) accounts a little more than the expected yield of two pyrrole rings and SnO_2 (22.9%) which indicate incomplete decomposition due to the presence of argon atmosphere.

On comparing the stability of complexes of thallium(III) and Sn(IV), complexes of later are expected to be more stable in the selected series of porphyrins. This is disclosed by the first decomposition temperature of 5-CSASnP2 at

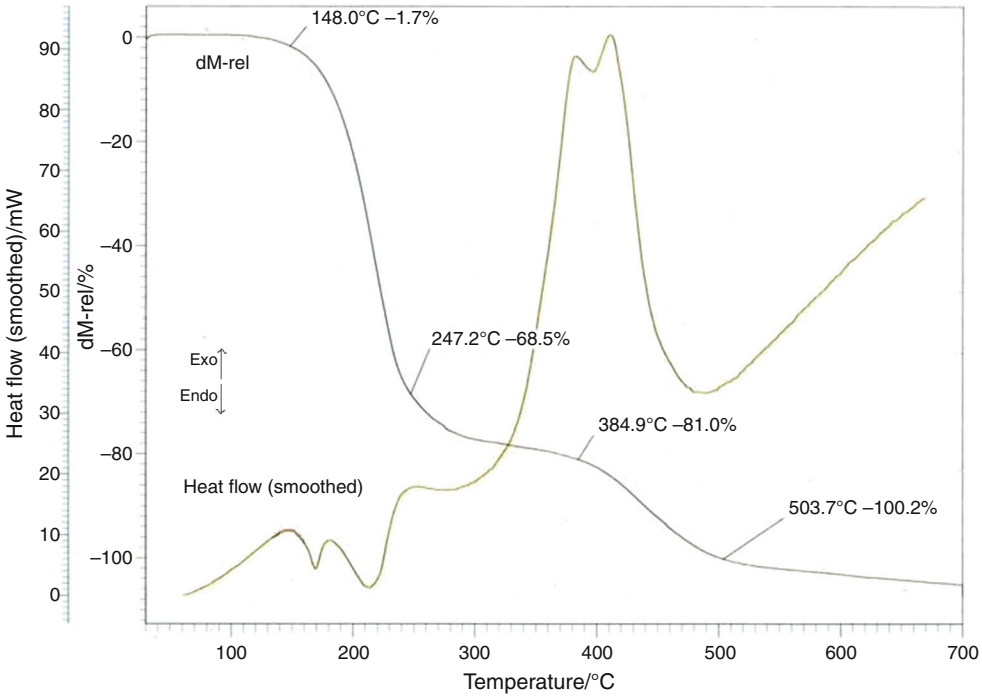

Fig. 1 TG/DTA curve of 5-CSATlP2

240 °C which is higher than the corresponding complex of thallium.

XRPD analysis

The crystallinity and phase of the product were examined by powdered XRD analysis. Figures 3 and 4 depict the XRD patterns of the P2, TlP2, SnP2, 5-CSATlP2 and 5-CSASnP2 with well-defined crystalline peaks indicating that the complex was amorphous in nature [18]. The experimental XRD pattern of complexes agrees with the JCPDS card no. 21-1272 (anatase phase) and the XRD pattern of rutile phases. The 2θ at 25.04°, 37.62°, 46.07°, 57.52° and 61.66° in the XRD pattern of 5-CSASnP2

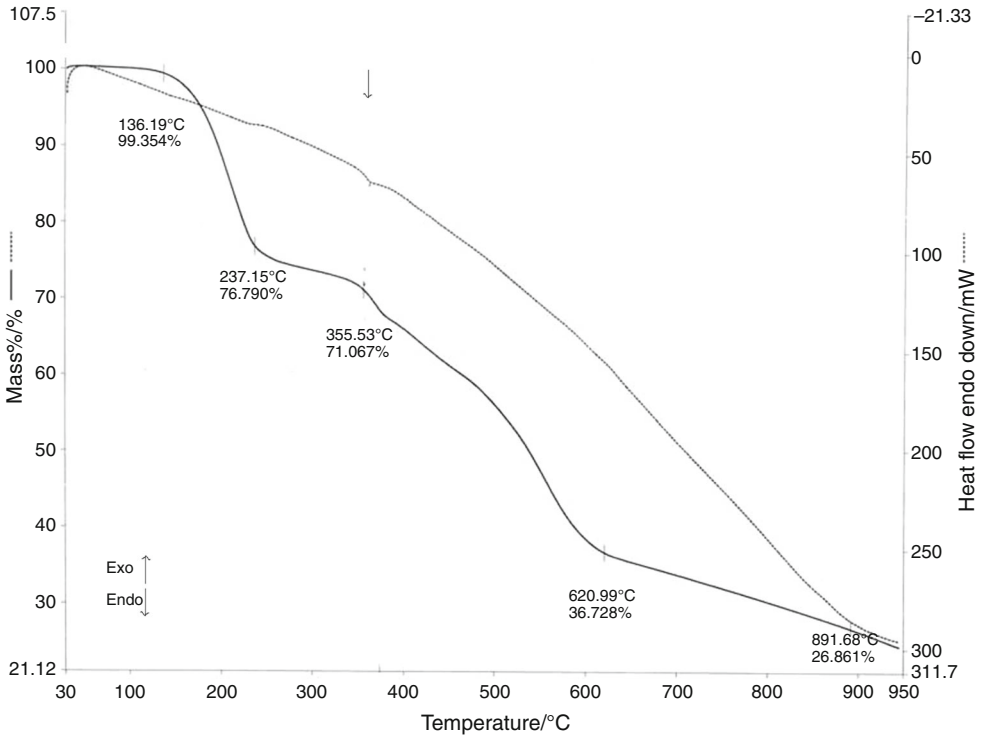

Fig. 2 TG/DTA curve of 5-CSASnP2

corresponding to the anatase phase [19], whereas 2θ values at 26.56°, 36.06°, 43.41°, 64.74° and 68.7° corresponding to the rutile phase with JCPDS card no. 21-1276 [20, 21]. Moreover, careful observation revealed that a systematic shift to the higher 2θ for the diffraction peaks of SnP2 and 5-CSASnP2 as compared to the base compound P2 (Fig. 3a, b). In the final complexes, the slight shift of diffraction lines toward right when compare with base compound is due to the metallation and axial ligation. The diffraction peaks of thallium complexes are little sharper than the XRD patterns of the tin complexes as a result of better crystallinity. The crystallite size of the complex d_{XRD} is estimated from XRD patterns using the Scherre's formula:

$$d_{XRD} = 0.9\lambda/\beta(\cos\theta)$$

d_{XRD} = crystallite size, λ = X-ray wavelength (1.54056 Å), β = full width at half maximum (FWHM) of the diffraction peak (radian), θ = diffraction angle at the peak maximum.

All the major peaks were used to calculate the average crystallite size of compounds. The XRD analysis shows that the P2, TlP2, SnP2, 5-CSATlP2 and 5-CSASnP2 had the average crystallite size of 32.41, 47.61, 35.90, 46.82 and 111.84 nm, respectively, confirming the nanocrystalline nature of the complexes. The observed line broadening in X-ray diffraction lines agrees well with the crystallite size of the above complexes. Sharper XRD peaks of 5-CSATlP2 (Fig. 4c) are typically indicative of high nanocrystalline nature and larger crystallite materials as is confirmed from its crystallite size calculations.

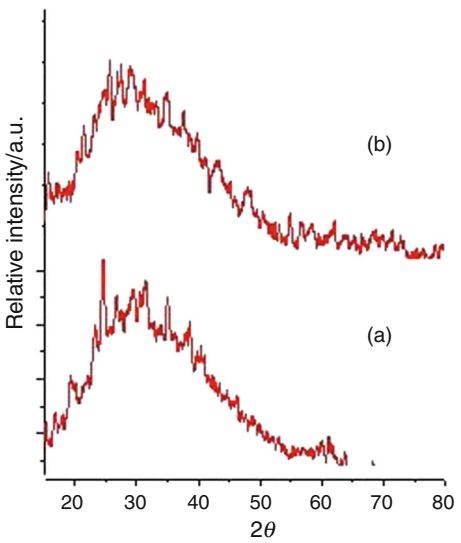

Fig. 3 PXRD pattern of (*a*) P2 (*b*) TlP2, (*b*) 5-CSATlP2

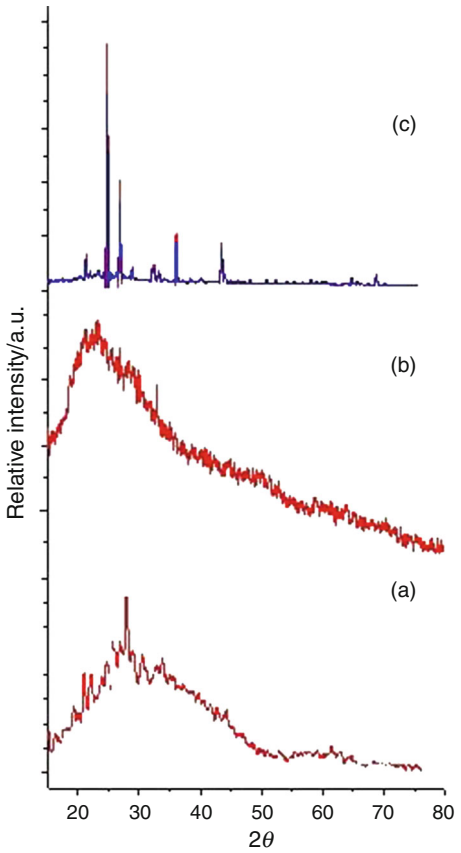

Fig. 4 PXRD pattern of (*a*) SnP2, (*b*) 5-CSASnP2

Fluorescence spectra and lifetime decay

The comparison of the fluorescence spectra resulting from excitation of the complexes 5-CSASnP2 and 5-CSATlP2 near the Soret bands is shown in Figs. 5 and 6. When excited at 425 nm, each complex gave a two-banded fluorescence spectrum in CH_2Cl_2. The λ_{em} values for tin complex are in the range of 597–611 (band I) and 650–660 nm (band II) which corresponds to the $S_1 \rightarrow S_0$ transition and the spectral profile is comparable with hexacoordinated tin(IV) porphyrin systems [2]. In thallium porphyrin complexes, the two emission bands observed at 652–672 and 700–725 nm correspond to the $S_1 \rightarrow S_0$ transition. Also, there is very weak emission at 647–650 nm which may correspond to the $S_2 \rightarrow S_0$ transition. As shown in the figure, the emission bands of tin porphyrins are less intense than thallium porphyrins which are attributed to the strong metal–ligand interaction in tin complexes in contrast to thallium complexes as is usually observed in case of in-plane porphyrins [22]. The red shift and the broadening in the fluorescence spectrum of thallium porphyrin complexes in comparison with the tin complex are due to the distortion of the macrocycles as is usually observed in SAT porphyrin complexes [23].

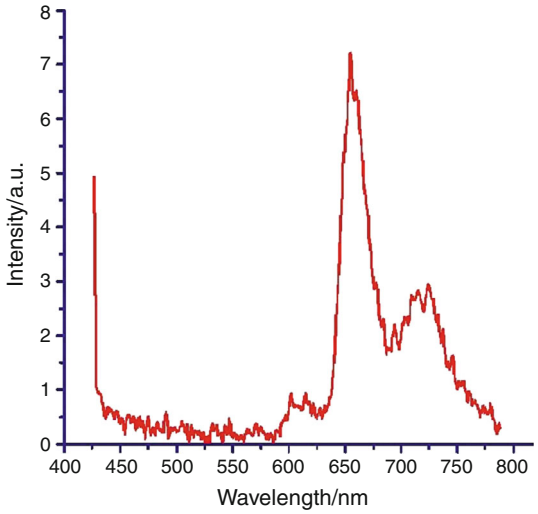

Fig. 5 Fluorescence spectra of 5-CSATlP2

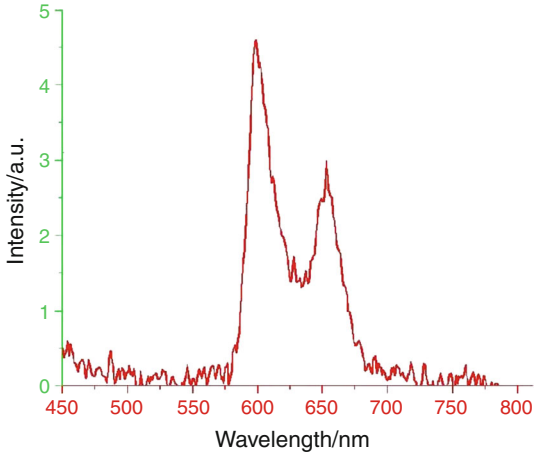

Fig. 6 Fluorescence spectra of 5-CSASnP2

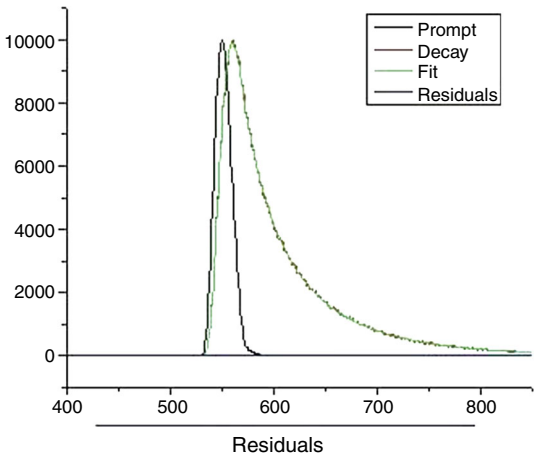

Fig. 7 Fluorescence decay and prompt instrumental response with λ_{exc} 425 nm of 5-CSATlP2 in CH_2Cl_2

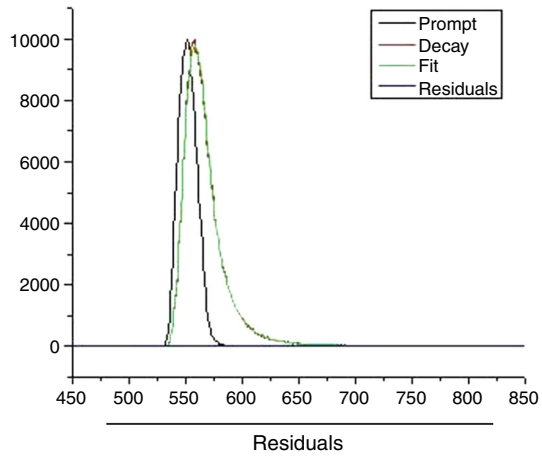

Fig. 8 Fluorescence decay and prompt instrumental response with λ_{exc} 425 nm of 5-CSASnP2 in CH_2Cl_2

The S_2-fluorescence decay profiles of 5-CSATlP2 and 5-CSASnP2 are illustrated in Figs. 7 and 8 from which S_2-state lifetimes of 5-CSATlP2 and 5-CSASnP2 were determined to be 0.44 and 0.55 ns, respectively.

Conclusions

In conclusion, we have synthesized various axially ligated metalloporphyrins with tin and thallium metals with different axial ligands and are well studied with UV–Vis, IR, TG, NMR, fluorescence and XRPD results. The optical absorption spectra reveal very large red shift effects and broadening of the absorption energies in response to the substitution of metal and axial ligands. The enhancement of the optical absorption is most pronounced in the long-wavelength visible region. Thermal studies of these compounds were performed trying to appreciate the thermal stability of these compounds and various thermal events of decompositions. The decomposition temperature of the respective porphyrins depends upon the metal-porphyrin bond strength in metalloporphyrins and cleavage of N–H bond in free-base porphyrin. XRPD studies reveal the phase and morphology of complexes, and the complexes are crystallized in mixed anatase, and rutile forms with well-defined crystalline peaks. What is more, the complexes produce strong characteristic fluorescence. Thus, the complexes of tin and thallium may be used as optical materials. The lifetimes of the S_2 state of the complexes obtained confirm previous measurements and permit accurate evaluations.

Acknowledgements We would like to acknowledge Indian Institute of Technology, Mandi, Himachal Pradesh, for photoluminescence studies and IIIM, Jammu, for their UV–Vis. studies. We thank University Grant Commission, New Delhi, for their support. We also thank IISC, Bangalore, for the NMR studies.

References

1. Auwarter W, Ecija D, Klappenberger F, Barth JV. Porphyrins at interfaces. Nat Chem. 2015;7:105.
2. Manke AM, Geisel K, Fetzer A, Kurz P. A water-soluble tin(IV) porphyrin as a bioinspired photosensitiser for light-driven proton-reduction. Phys Chem Chem Phys. 2014;16:12029.
3. Desbois N, Pacquelet S, Dubois A, Michelin C, Gros CP. Easy access to heterobimetallic complexes for medical imaging applications via microwave-enhanced cycloaddition. Beilstein J Org Chem. 2015;11:2202.
4. Calvete MJF, Simoes AVC, Henriques CA, Pinto SMA, Pereira MM. Tetrapyrrolic macrocycles: potentialities in medical imaging technologies. Curr Org Synth. 2014;11:1.
5. Rayati S, Nejabat F. Preparation of porphyrin nanoparticles: effect of bromine atom on the particle size and catalytic activity. Inorg Chem Commun. 2016;70:172.
6. Marijuan AF, Barandika G, Baza B, Urtiagaa M, Arriortua MI. Thermal stability and crystallochemical analysis for Co(II)—based coordination polymers with TPP and TPPS porphyrins. Cryst Eng Commun. 2013;15:4181.
7. Bogdan ML, Zgierski MZ, Bischoff C, Li M, Hu MY, Zhao J, Martin SW, Alp EE, Scheidt WR. Quantitative vibrational dynamics of the metal site in a tin porphyrin: an IR, NRVS, and DFT study. Inorg Chem. 2013;52:9948–53.
8. Gharaati S, Moghadamb M, Tangestaninejad S, Mirkhani V, Mohammadpoor-Baltork I, Barati B, Sadegh F. High-valent tin(IV) porphyrins: efficient and selective catalysts for cyclopropanation of styrene derivatives with EDA under mild conditions. J Organomet Chem. 2013;741–742:78–82.
9. Chen Y, Li A, Huang ZH, Wang LN, Kang F. Porphyrin-based nanostructures for photocatalytic applications. Nanomaterials. 2016;6:51.
10. Valicsek Z, Horvath O. Formation, photophysics and photochemistry of thallium(III) 5,10,15,20-tetrakis(4-sulphonatophenyl)porphyrin: new supports of typical sitting-atop features. J Photochem Photobiol A Chem. 2007;186:1.
11. Horvath O, Huszank R, Valicsek Z, Lendvay G. Photophysics and photochemistry of kinetically labile, water-soluble porphyrin complexes. Coord Chem Rev. 2006;250:1792.
12. Valicsek Z, Horváth O, Lendvay G, Kikăs I, Škorić I. Formation, photophysics, and photochemistry of cadmium(II) complexes with 5,10,15,20-tetrakis(4-sulfonatophenyl) porphyrin and its octabromo derivative: the effects of bromination and the axial hydroxo ligand. J Photochem Photobiol A Chem. 2011;218:143–55.
13. Valicsek Z, Horvath O, Patonay K. Formation, photophysical and photochemical properties of water-soluble bismuth(III) porphyrins: the role of the charge and structure. J Photochem Photobiol A Chem. 2011;226:23.
14. Ren DM, Guo Z, Du F, Liu ZF, Zhou ZC, Shi XY, Chen YS, Zheng JY. A novel soluble tin(IV) porphyrin modified single-walled carbon nanotube nanohybrid with light harvesting properties. Int J Mol Sci. 2008;9:45.
15. Kim HJ, Park KM, Ahn TK, Kim SK, Kim KS, Kim D, Kim HJ. Novel fullerene-porphyrin-fullerene triad linked by metal axial coordination: synthesis, X-ray crystal structure, and spectroscopic characterizations of trans-bis([60]fullerenoacetato)tin(IV) porphyrin. Chem Commun. 2004;. doi:10.1039/b411482.
16. Bajju GD, Katoch S, Devi G, Kundan S, Ashu K, Bhagat M. Synthesis and characterization of some new thallium(III) macrocyclic complexes and their biological studies. Main Group Met Chem. 2016;39:19.
17. Shetti VS, Ravikanth M. A simple alternative method for preparing Sn(IV) porphyrins. J Porphyr Phthalocyanines. 2010;14:361.
18. Chandraleka S, Chandramohan G. Afr J Pure Appl Chem. 2014;8:162.
19. Rahimi R, Fard EH, Saadati S, Rabbani M. Degradation of methylene blue via Co–TiO_2 nano powders modified by meso-tetra(carboxyphenyl) porphyrin. J Sol-Gel Sci Technol. 2012;62:351.
20. Miao L, Jin P, Kaneko K, Terai A, Gabain NN, Tanemura S. Preparation and characterization of polycrystalline anatase and rutile TiO_2 thin films by rf magnetron sputtering. Appl Surf Sci. 2003;212:255.
21. Francisco MSP, Mastelaro VR. Inhibition of the anatase–rutile phase transformation with addition of CeO_2 to CuO–TiO_2 system: Raman spectroscopy, X-ray diffraction, and textural studies. Chem Mater. 2002;14:2514.
22. Major MM, Horvath O, Fodor MA, Fodor L, Valicsek Z, Gramp G, Wankmüller A. Photophysical and photocatalytic behavior of nickel(II) 5,10,15,20-tetrakis(1-methylpyridinium-4-yl)porphyrin. Inorg Chem Commun. 2016;73:1.
23. Horvath O, Valicsek Z, Harrach G, Lendvay G, Fodor MA. Spectroscopic and photochemical properties of water-soluble metalloporphyrins of distorted structure. Coord Chem Rev. 2012;256:1531.